

Supplement of Atmos. Chem. Phys., 18, 289–309, 2018
<https://doi.org/10.5194/acp-18-289-2018-supplement>
© Author(s) 2018. This work is distributed under
the Creative Commons Attribution 4.0 License.



Atmospheric
Chemistry
and Physics
Open Access
EGU

Supplement of

Quantifying black carbon light absorption enhancement with a novel statistical approach

Cheng Wu et al.

Correspondence to: Cheng Wu (wucheng.vip@foxmail.com) and Jian Zhen Yu (jian.yu@ust.hk)

The copyright of individual parts of the supplement might differ from the CC BY 4.0 License.

This SI contains five tables and twenty-five figures.

Uncertainty of E_{abs} estimation

The uncertainty of E_{abs} estimation depends on uncertainty propagation from MAE uncertainty, which can be calculated from (Harris, 2010):

$$MAE_{Unc} = MAE \times \sqrt{\left(\frac{\sigma_{abs,Unc}}{\sigma_{abs}}\right)^2 + \left(\frac{EC_{Unc}}{EC}\right)^2} \quad S1$$

$$E_{abs,Unc} = E_{abs} \times \sqrt{\left(\frac{MAE_{Unc}}{MAE}\right)^2 + \left(\frac{MAE_{p,Unc}}{MAE_p}\right)^2} \quad S2$$

Descriptions of customized programs used in this study for data analysis and visualization

Several computer programs were developed to meet specific research purpose in this study. All the programs are based on Igor Pro (www.wavemetrics.com) that provides a friendly GUI. Brief descriptions are given below.

MRS program (Igor Pro based)

The program (Figure S21) is written in Igro Pro (WaveMetrics, Inc. Lake Oswego, OR, USA) to feasible MRS calculation via a user-friendly GUI. The MRS application is not limited in SOC estimation, but can also be extended to other applications (e.g. E_{abs} estimation) as long as a reliable tracer is available.

MRS calculation can be done by different temporal cycles (batch calculation): by year, by year&season, by season, by year&month, by month, by year&month&hour. Data filter is also available to calculate MRS on a specific subset of data.

The program is available from <https://sites.google.com/site/wuchengust>.

Mie program and source code written in Igor Pro

A computer program (Figure S22) written in Igro Pro (WaveMetrics, Inc. Lake Oswego, OR, USA) for Mie scattering calculation. Both BHMIE and BHCOAT (coated particles) algorithms(Bohren and Huffman, 1983) are included. The program is also capable of batch calculation for both algorithms. Available from <https://sites.google.com/site/wuchengust>.

Aethalometer data processing program (Igor Pro based)

This handy tool (Figure S23) can perform different corrections (e.g. Weingartner, Virkkula) on Aethalometer data. Raw Aethalometer data suffers from several artifacts including filter matrix effect (multiple scattering), loading effect (shadowing) and scattering effect. Careful corrections are needed for reporting light absorption coefficient from attenuation measurement. This Igor based program can directly import Aethalometer raw data and perform corrections (algorithm can be selected by user). Results can be exported to .csv files. Extra information including statistics of sensor voltage from each channel, sampling flow rate, etc are plotted for a quick QA/QC check. Available from <https://sites.google.com/site/wuchengust>.

Histbox program (Igor Pro based)

A handy tool (Figure S24) to generate histogram and box plots with many powerful features. Data can be sorted by different time scale and batch plotting is available. Available from <https://sites.google.com/site/wuchengust>.

Scatter plot program (Igor Pro based)

Scatter plot (Figure S25) is a useful tool to maximize the efficiency of data visualization in atmospheric science. The program includes Deming, WODR and York algorithm for linear regression, which consider uncertainties in both X and Y, that is more realistic for atmospheric applications (Wu and Yu, 2017). It is Igor based, and packed with lots of useful features for data analysis and graph plotting, including batch plotting, data masking via GUI, color coding in Z axis, data filtering and grouping. Available from <https://sites.google.com/site/wuchengust>.

References

- Andreae, M. O., Schmid, O., Yang, H., Chand, D., Yu, J. Z., Zeng, L. M., and Zhang, Y. H.: Optical properties and chemical composition of the atmospheric aerosol in urban Guangzhou, China, *Atmos. Environ.*, 42, 6335-6350, doi: 10.1016/j.atmosenv.2008.01.030, 2008.
- Bohren, C. F. and Huffman, D. R.: *Absorption and scattering of light by small particles*, Wiley, New York, xiv, 530 p. pp., 1983.
- Chan, T. W., Brook, J. R., Smallwood, G. J., and Lu, G.: Time-resolved measurements of black carbon light absorption enhancement in urban and near-urban locations of southern Ontario, Canada, *Atmos. Chem. Phys.*, 11, 10407-10432, doi: 10.5194/acp-11-10407-2011, 2011.
- Chow, J. C., Watson, J. G., Doraiswamy, P., Chen, L. W. A., Sodeman, D. A., Lowenthal, D. H., Park, K., Arnott, W. P., and Motallebi, N.: Aerosol light absorption, black carbon, and elemental carbon at the Fresno Supersite, California, *Atmos. Res.*, 93, 874-887, doi: 10.1016/j.atmosres.2009.04.010, 2009.
- Chuang, P. Y., Duvall, R. M., Bae, M. S., Jefferson, A., Schauer, J. J., Yang, H., Yu, J. Z., and Kim, J.: Observations of elemental carbon and absorption during ACE-Asia and implications for aerosol radiative properties and climate forcing, *J. Geophys. Res.*, 108, 8634, doi: 10.1029/2002jd003254, 2003.
- Doran, J. C., Barnard, J. C., Arnott, W. P., Cary, R., Coulter, R., Fast, J. D., Kassianov, E. I., Kleinman, L., Laulainen, N. S., Martin, T., Paredes-Miranda, G., Pekour, M. S., Shaw, W. J., Smith, D. F., Springston, S. R., and Yu, X. Y.: The T1-T2 study: evolution of aerosol properties downwind of Mexico City, *Atmos. Chem. Phys.*, 7, 1585-1598, doi: 10.5194/acp-7-1585-2007, 2007.
- Harris, D. C.: Quantitative chemical analysis, 8th ed., W.H. Freeman and Co., New York, 2010.
- Knox, A., Evans, G. J., Brook, J. R., Yao, X., Jeong, C. H., Godri, K. J., Sabaliauskas, K., and Slowik, J. G.: Mass Absorption Cross-Section of Ambient Black Carbon Aerosol in Relation to Chemical Age, *Aerosol. Sci. Technol.*, 43, 522-532, doi: 10.1080/02786820902777207, 2009.
- Lack, D. A. and Cappa, C. D.: Impact of brown and clear carbon on light absorption enhancement, single scatter albedo and absorption wavelength dependence of black carbon, *Atmos. Chem. Phys.*, 10, 4207-4220, doi: 10.5194/acp-10-4207-2010, 2010.
- Lan, Z.-J., Huang, X.-F., Yu, K.-Y., Sun, T.-L., Zeng, L.-W., and Hu, M.: Light absorption of black carbon aerosol and its enhancement by mixing state in an urban atmosphere in South China, *Atmos. Environ.*, 69, 118-123, doi: 10.1016/j.atmosenv.2012.12.009, 2013.
- Liu, D., Flynn, M., Gysel, M., Targino, A., Crawford, I., Bower, K., Choularton, T., Jurányi, Z., Steinbacher, M., Hüglin, C., Curtius, J., Kampus, M., Petzold, A., Weingartner, E., Baltensperger, U., and Coe, H.: Single particle characterization of black carbon aerosols at a tropospheric alpine site in Switzerland, *Atmos. Chem. Phys.*, 10, 7389-7407, doi: 10.5194/acp-10-7389-2010, 2010.
- Mayol-Bracero, O. L., Gabriel, R., Andreae, M. O., Kirchstetter, T. W., Novakov, T., Ogren, J., Sheridan, P., and Streets, D. G.: Carbonaceous aerosols over the Indian Ocean during the Indian Ocean Experiment (INDOEX): Chemical characterization, optical properties, and probable sources, *J. Geophys. Res.*, 107, 8030, doi: 10.1029/2000jd000039, 2002.
- Moosmüller, H., Chakrabarty, R. K., Ehlers, K. M., and Arnott, W. P.: Absorption Angstrom coefficient, brown carbon, and aerosols: basic concepts, bulk matter, and spherical particles, *Atmos. Chem. Phys.*, 11, 1217-1225, doi: 10.5194/acp-11-1217-2011, 2011.
- Naoe, H., Hasegawa, S., Heintzenberg, J., Okada, K., Uchiyama, A., Zaizen, Y., Kobayashi, E., and Yamazaki, A.: State of mixture of atmospheric submicrometer black carbon particles and its effect on particulate light absorption, *Atmos. Environ.*, 43, 1296-1301, doi: 10.1016/j.atmosenv.2008.11.031, 2009.

- Pandolfi, M., Cusack, M., Alastuey, A., and Querol, X.: Variability of aerosol optical properties in the Western Mediterranean Basin, *Atmos. Chem. Phys.*, 11, 8189-8203, doi: 10.5194/acp-11-8189-2011, 2011.
- Thompson, J. E., Hayes, P. L., Jimenez, K. A. J. L., Zhang, X., Liu, J., Weber, R. J., and Buseck, P. R.: Aerosol Optical Properties at Pasadena, CA During CalNex 2010, *Atmos Environ*, doi: 10.1016/j.atmosenv.2012.03.011, 2012.
- Wang, Q., Huang, R., Zhao, Z., Cao, J., Ni, H., Tie, X., Zhu, C., Shen, Z., Wang, M., and Dai, W.: Effects of photochemical oxidation on the mixing state and light absorption of black carbon in the urban atmosphere of China, *Environmental Research Letters*, 12, 044012, 2017.
- Wang, Q. Y., Huang, R. J., Cao, J. J., Han, Y. M., Wang, G. H., Li, G. H., Wang, Y. C., Dai, W. T., Zhang, R. J., and Zhou, Y. Q.: Mixing State of Black Carbon Aerosol in a Heavily Polluted Urban Area of China: Implications for Light Absorption Enhancement, *Aerosol. Sci. Technol.*, 48, 689-697, doi: 10.1080/02786826.2014.917758, 2014.
- Wu, C. and Yu, J. Z.: Evaluation of linear regression techniques for atmospheric applications: The importance of appropriate weighting, *Atmos. Meas. Tech. Discuss.*, 2017, 1-31, doi: 10.5194/amt-2017-300, 2017.
- Xu, J., Bergin, M. H., Yu, X., Liu, G., Zhao, J., Carrico, C. M., and Baumann, K.: Measurement of aerosol chemical, physical and radiative properties in the Yangtze delta region of China, *Atmos. Environ.*, 36, 161-173, doi: 10.1016/S1352-2310(01)00455-1, 2002.
- Yang, M., Howell, S. G., Zhuang, J., and Huebert, B. J.: Attribution of aerosol light absorption to black carbon, brown carbon, and dust in China - interpretations of atmospheric measurements during EAST-AIRE, *Atmos. Chem. Phys.*, 9, 2035-2050, doi: 10.5194/acp-9-2035-2009, 2009.

Table S1. Comparison of Mass absorption efficiency (MAE) at various locations. For literature MAE values at different wavelengths rather than 550 nm, an estimated MAE₅₅₀ is given in the brackets following equations given by Moosmuller et al. (2011) assuming AAE of 1.

Location	Type	Sampling Duration	Inlet	λ (nm)	σ_{abs} Instrument	EC determination protocol	$\sigma_{abs} \pm 1$ S.D. (Mm ⁻¹)	EC mass ($\mu\text{g m}^{-3}$)	estimated MAE _p (m ² g ⁻¹)			observed MAE (m ² g ⁻¹) arithmetic mean ± 1 S.D.	Gaussian fit	Reference
									MAE _p (m ² g ⁻¹)	arithmetic mean ± 1 S.D.	Gaussian fit			
Guangzhou, China	Suburban	2012.2-2013.1	PM _{2.5}	550	AE	NIOSH_TOT	42.65 \pm 29.41	2.66 \pm 2.27	13*	18.75 \pm 6.16	16.16	This study		
Shenzhen, China	Urban	2011.8-9	PM _{2.5}	532	PAS	LII	25.4 \pm 19.0	4.0 \pm 3.1	/	6.5 \pm 0.5[6.29 \pm 0.48]	/	(Lan et al., 2013)		
Xi'an, China	Urban	2012.12-2013.1	PM _{2.5}	870	PAS	LII	/	8.8 \pm 7.3	7.17[11.34]	/	7.62[12.05]	(Wang et al., 2014)		
Xi'an, China	Urban	2013.2	PM _{2.5}	532	PAS	LII				14.6 \pm 5.6	12.7	(Wang et al., 2017)		
Guangzhou, China	Urban	2004.10	PM _{2.5}	532	PAS	NIOSH_TOT	91 \pm 60	7.1	7.7[7.44]	/	/	(Andreae et al., 2008)		
Fresno, USA	Urban	2005.8-9	PM _{2.5}	532	PAS	IMPROVE_A_TOR	5.06	1.01	/	6.1 \pm 2.5[5.9 \pm 2.42]	/	(Chow et al., 2009)		
						NIOSH_TOT		0.58	/	9.3 \pm 2.4[8.99 \pm 2.32]	/			
Tl, Mexico city, Mexico	Suburban	2006.3	PM _{2.5}	870	PAS	NIOSH_TOT	/	/	/	9.2 \sim 9.7***[14.55 \sim 15.34]	/	(Doran et al., 2007)		
Tokyo, Japan	Suburban	2005.8	PM _{2.5}	565	PSAP	IMPROVE_A_TOR	30.43 \pm 20.41	2.9 \pm 2.13	11 \pm 1	/	/	(Naoe et al., 2009)		
Pasadena, USA	Urban	2010.5-6	PM _{2.5}	532	AM	NIOSH_TOT	3.8 \pm 3.4	0.6 \sim 0.7	5.7[5.51]	/	/	(Thompson et al., 2012)		
Toronto, Canada	Urban	2006.12-2007.1	PM _{2.5}	760	PAS	NIOSH_TOT	/	/	6.9 \sim 9.1** [9.53 \sim 12.57]	9.3 \sim 9.9[12.85 \sim 13.68]	/	(Knox et al., 2009)		
Toronto, Canada	Suburban						3 \sim 6	0.10 \sim 0.14	/	30 \sim 43[42.6 \sim 61.06]	/			
Windsor, Canada	Urban	2007.8	PM _{2.5}	781	PAS	LII	4.4 \pm 2.9	0.27 \pm 0.23	/	16 \pm 1[22.72 \pm 1.42]	/	(Chan et al., 2011)		
Ottawa, Canada	Urban						26 \pm 17	1.7 \pm 0.9	/	15 \pm 3[21.3 \pm 4.26]	/			
Beijing, China	Rural	2005.3	/	550	AE	NIOSH_TOT	/	/	9.5	11.3	/	(Yang et al., 2009)		
Montserrat, Spain	Rural (Mediterranean)	2009.11-2010.10	PM ₁₀	637	MAAP	NIOSH_TOT	2.8 \pm 2.2	0.271 \pm 0.2 15	/	10.4[12.04]	/	(Pandolfi et al., 2011)		
Jungfraujoch, Switzerland	Rural (high alpine)	2007.2-3	/	637	MAAP	LII	/	/	/	10.2 \pm 3.2[11.81 \pm 3.71]	/	(Liu et al., 2010)		
Lin'an, China	Rural	1999.11	PM _{2.5}	550	PSAP	NIOSH_TOT	23 \pm 14	3.4 \pm 1.7	/	8.6 \pm 7.0	/	(Xu et al., 2002)		
Jeju Island, Korea	Coastal Rural, (East China Sea)	2001.4	PM ₁₀	550	PSAP	NIOSH_TOT	/	/	/	12.6 \pm 2.6	/	(Chuang et al., 2003)		
Maldives	Oceanic rural	1999.2-3	PM ₃	550	PSAP	EGA	62 \pm 34	2.5 \pm 1.4	6.6	8.1	/	(Mayol-Bracero et al., 2002)		

*Determined by Minimum R Squared method; ** Median values;

AE:Aethalometer ; PAS photo acoustic spectrometer; MAAP: Multi Angle Absorption Photometer; PSAP: particle soot absorption photometer; AM: albedo meter; LII: Laser induced incandescence

Table S2. Statistics of monthly MAE₅₅₀ (m²g⁻¹).

Month	95th	75th	50th	25th	5th	Mean	Max	Min	S.D.	N
Feb-2012	31.24	22.00	18.12	15.74	13.92	19.66	47.73	11.74	5.66	529
Mar-2012	26.51	19.63	17.45	15.91	13.71	18.46	45.56	10.98	4.30	651
Apr-2012	33.06	22.66	18.24	16.11	13.85	20.21	48.29	6.01	6.23	595
May-2012	33.24	23.25	19.59	17.16	14.82	21.07	46.66	6.33	5.62	528
Jun-2012	35.52	25.86	21.28	18.57	14.99	22.95	49.07	5.62	6.66	315
Jul-2012	33.93	23.77	18.81	15.58	12.71	20.51	49.22	9.23	6.79	587
Aug-2012	40.75	27.72	21.85	16.14	12.51	23.09	49.95	9.75	8.56	545
Sep-2012	30.75	20.86	17.52	15.24	12.97	18.99	46.44	10.39	5.63	674
Oct-2012	20.72	15.84	13.95	12.60	11.18	14.70	34.09	7.34	3.21	715
Nov-2012	26.45	18.10	15.43	13.70	11.89	16.75	39.32	8.34	4.72	495
Dec-2012	28.57	19.04	15.73	13.66	11.78	17.18	47.39	9.33	5.47	585
Jan-2013	21.53	16.24	14.47	13.03	11.80	15.29	43.19	7.16	3.77	708

Table S3. Statistics of monthly AAE₄₇₀₋₆₆₀.

Month	95th	75th	50th	25th	5th	Mean	Max	Min	S.D.	N
Feb-2012	1.42	1.26	1.18	1.11	0.96	1.19	1.72	0.86	0.14	529
Mar-2012	1.33	1.18	1.10	1.02	0.93	1.10	1.50	0.65	0.12	651
Apr-2012	1.19	1.08	1.02	0.95	0.78	1.01	1.76	0.15	0.14	595
May-2012	1.13	1.05	1.00	0.94	0.84	0.99	1.24	0.39	0.10	528
Jun-2012	1.18	1.10	1.04	0.97	0.90	1.04	1.29	0.78	0.09	315
Jul-2012	1.22	1.11	1.04	0.98	0.83	1.04	1.43	0.20	0.13	587
Aug-2012	1.18	1.10	1.04	0.99	0.90	1.04	1.31	0.69	0.09	545
Sep-2012	1.23	1.13	1.06	1.00	0.91	1.07	1.40	0.64	0.11	674
Oct-2012	1.27	1.16	1.09	1.02	0.93	1.09	1.40	0.85	0.10	715
Nov-2012	1.24	1.16	1.11	1.05	0.97	1.11	1.52	0.79	0.08	495
Dec-2012	1.33	1.22	1.16	1.10	1.01	1.16	1.42	0.77	0.09	585
Jan-2013	1.38	1.27	1.18	1.12	1.01	1.19	1.66	0.93	0.11	708

Table S4. Statistics of monthly SSA₅₂₅.

Month	95th	75th	50th	25th	5th	Mean	Max	Min	S.D.	N
Feb-2012	0.91	0.89	0.87	0.84	0.79	0.86	0.94	0.65	0.04	526
Mar-2012	0.91	0.89	0.86	0.83	0.77	0.85	0.95	0.42	0.05	648
Apr-2012	0.92	0.89	0.86	0.83	0.76	0.85	0.94	0.45	0.06	552
May-2012	0.92	0.90	0.87	0.83	0.74	0.85	0.94	0.45	0.06	527
Jun-2012	0.92	0.89	0.86	0.81	0.74	0.84	0.95	0.64	0.06	310
Jul-2012	0.91	0.87	0.83	0.79	0.71	0.83	0.95	0.57	0.06	580
Aug-2012	0.94	0.92	0.89	0.85	0.79	0.88	0.96	0.67	0.05	536
Sep-2012	0.93	0.91	0.88	0.84	0.75	0.87	0.96	0.55	0.06	672
Oct-2012	0.94	0.93	0.91	0.89	0.84	0.90	0.96	0.66	0.03	715
Nov-2012	0.91	0.90	0.87	0.83	0.75	0.86	0.94	0.18	0.06	495
Dec-2012	0.91	0.89	0.86	0.82	0.74	0.85	0.94	0.66	0.05	585
Jan-2013	0.91	0.89	0.87	0.85	0.80	0.86	0.93	0.64	0.04	708

Table S5. Statistics of monthly E_{abs550}.

Month	95th	75th	50th	25th	5th	Mean	Max	Min	S.D.	N
Feb-2012	2.23	1.59	1.31	1.14	1.04	1.43	3.41	1.00	0.40	501
Mar-2012	1.76	1.30	1.15	1.07	1.02	1.24	2.83	1.00	0.26	466
Apr-2012	2.46	1.70	1.37	1.21	1.07	1.52	3.58	1.00	0.45	576
May-2012	2.48	1.73	1.45	1.28	1.12	1.57	3.46	1.02	0.41	520
Jun-2012	2.47	1.80	1.49	1.30	1.09	1.61	3.38	1.01	0.45	305
Jul-2012	2.83	1.97	1.57	1.30	1.10	1.71	4.03	1.01	0.55	568
Aug-2012	3.45	2.34	1.86	1.40	1.11	1.97	4.20	1.00	0.71	528
Sep-2012	2.36	1.62	1.36	1.20	1.05	1.48	3.54	1.00	0.42	636
Oct-2012	1.87	1.44	1.27	1.15	1.04	1.34	3.07	1.00	0.28	683
Nov-2012	2.14	1.51	1.27	1.13	1.04	1.38	3.17	1.00	0.38	461
Dec-2012	2.46	1.64	1.35	1.18	1.05	1.49	4.02	1.00	0.46	555
Jan-2013	1.85	1.39	1.24	1.12	1.03	1.31	3.66	1.00	0.32	672

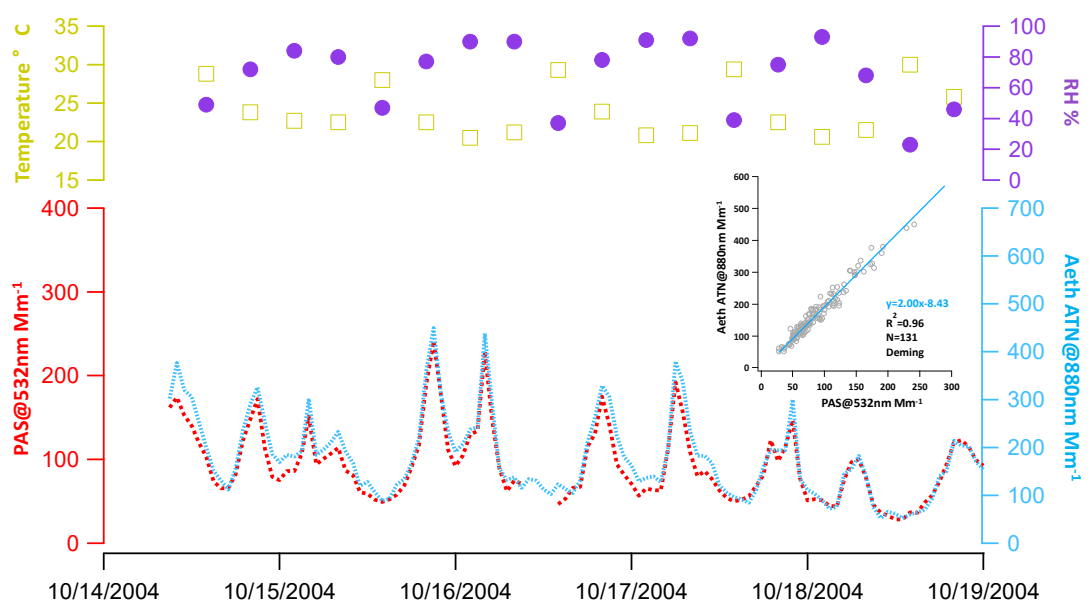


Figure S1. Comparison of collocated Aethalometer and PAS at Guangzhou (Oct 2004). Both PAS and Aethalometer (AE-16) were equipped with PM_{2.5} inlets. RH of the sampled air was controlled to be <45% for PAS. Aethalometer sampling was conducted without RH control.

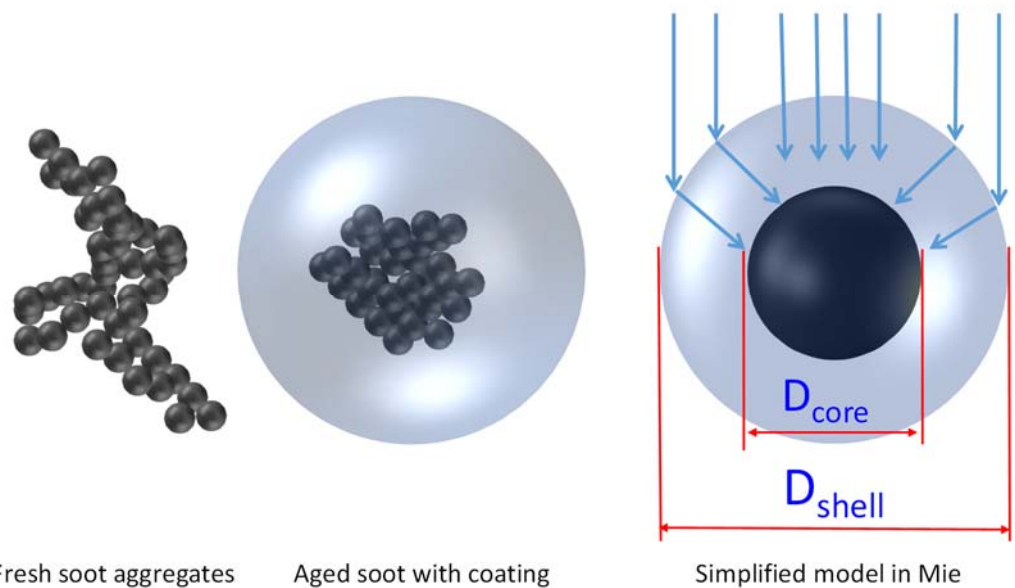


Figure S2. Schematic of the aging effect on light absorption. More light is absorbed by the soot particle core due to the lensing effect of the coating materials.

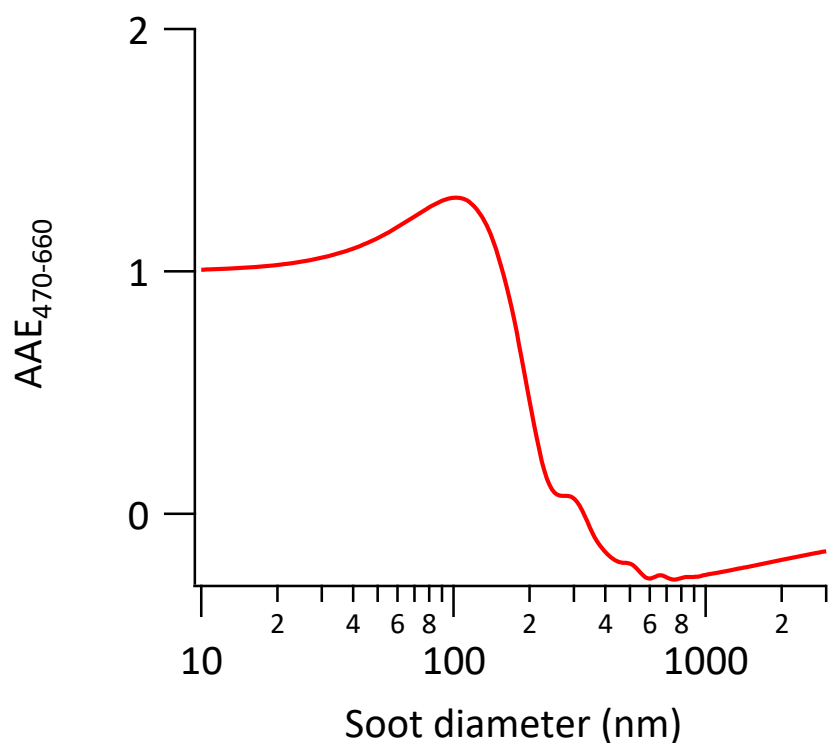


Figure S3. Mie simulated $\text{AAE}_{470-660}$ of a bare soot particle as a function of diameter with a Refractive index of $1.85 - 0.71i$.

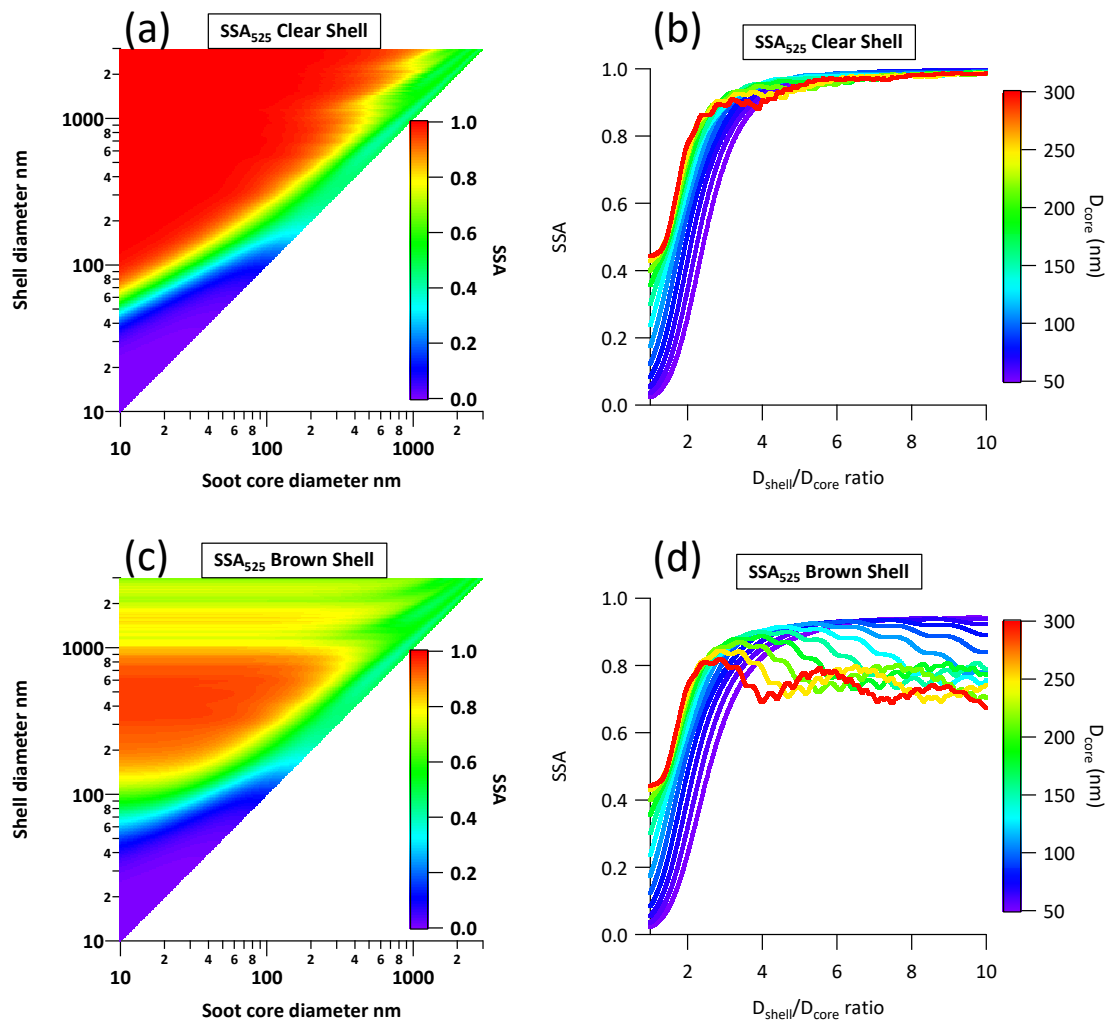


Figure S4. Mie simulated size dependency of soot particles SSA at wavelength 525 nm. (a) Combination of different clear shell (y axis) and core diameters (x axis). The color coding represents the SSA of a particle with specific core and clear shell size; (b) Cross-sections views of (a). The color coding represents different D_{core} in the range of 50 – 300 nm. (c)&(d) Similar to (a)&(b) but from the brown shell scenario.

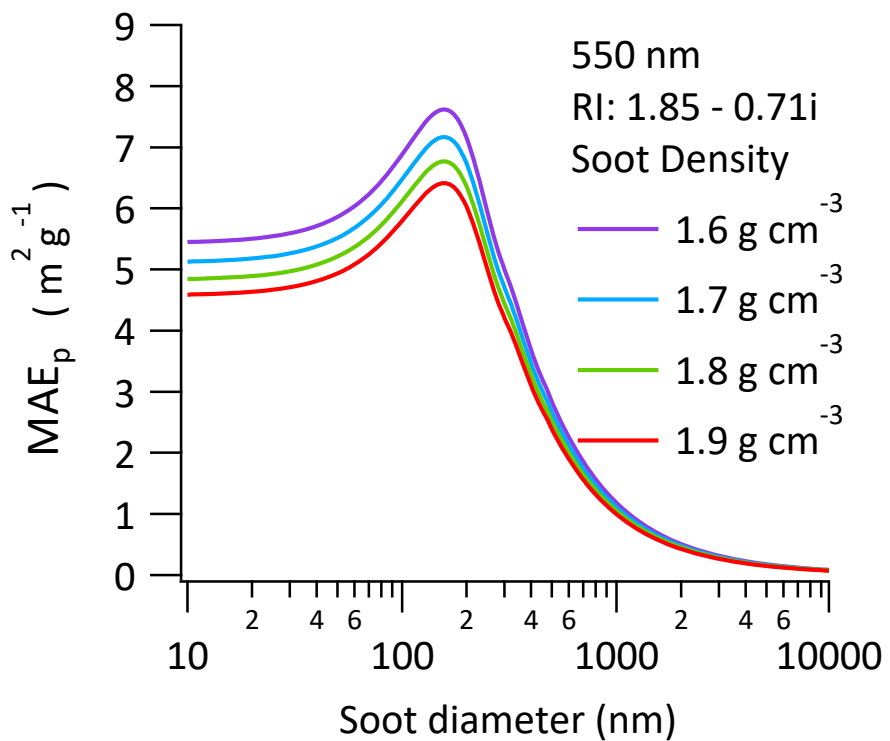


Figure S5. Mie simulated mass absorption efficiency (MAE_p) of a bare soot particle as a function of diameter at a wavelength of 550nm. Refractive index is $1.85 - 0.71i$ and density varied from 1.6 to 1.9 g cm^{-3} .

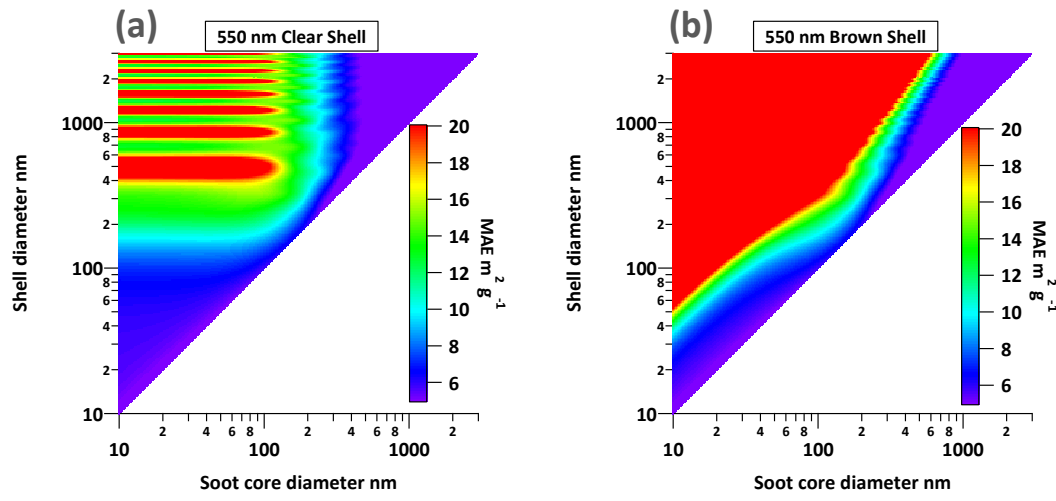


Figure S6. Mie simulated mass absorption efficiency (MAE) of a bare soot particle as a function of diameter at a wavelength of 550nm. Refractive index is $1.85 - 0.71i$ and density is 1.9 g cm^{-3} for the soot core. Refractive index for clear coating is 1.55. Refractive index for brown coating is wavelength dependent adopted from Lack and Cappa (2010).

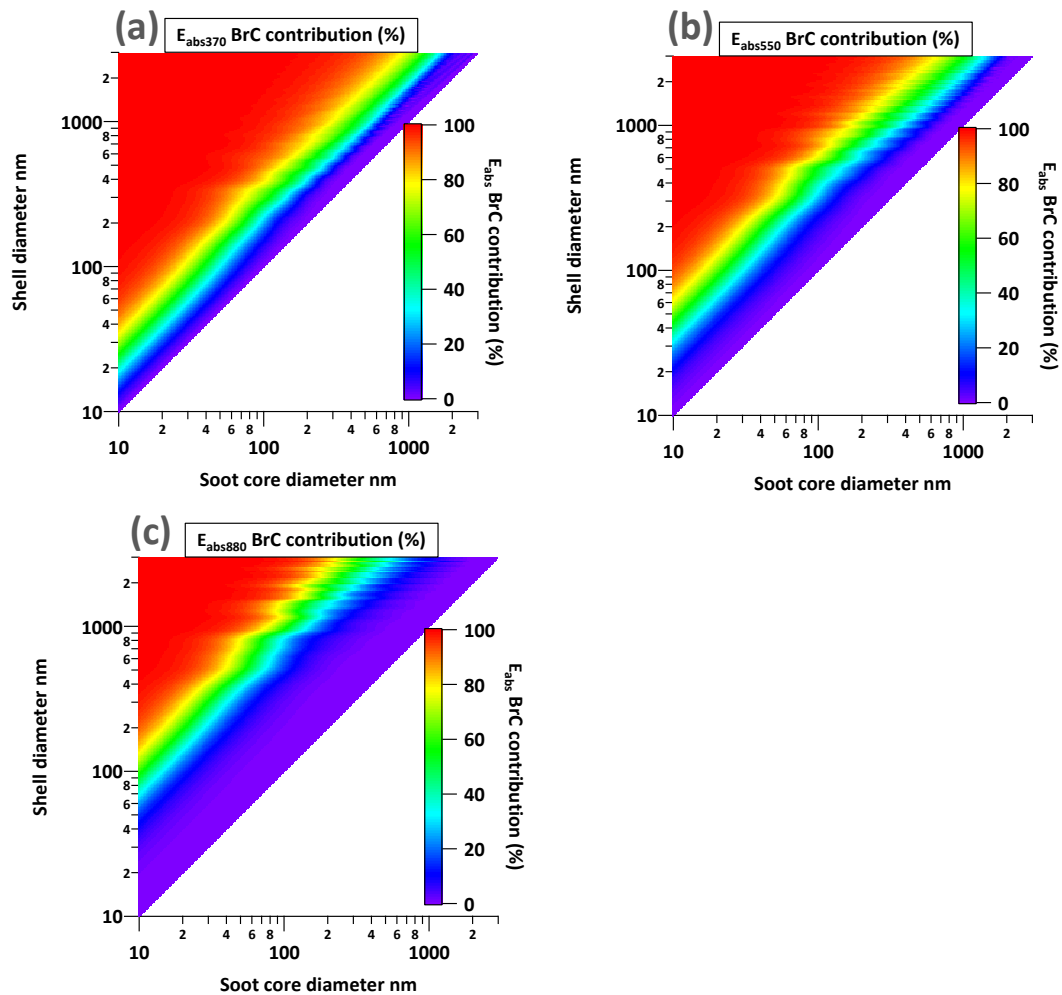


Figure S7. Mie simulated BrC absorption contribution to total E_{abs} (lensing effect + BrC absorption) in the brown shell scenario. The color coding represents fractional absorption contribution from BrC. (a) 370 nm (b) 550 nm (c) 880 nm.

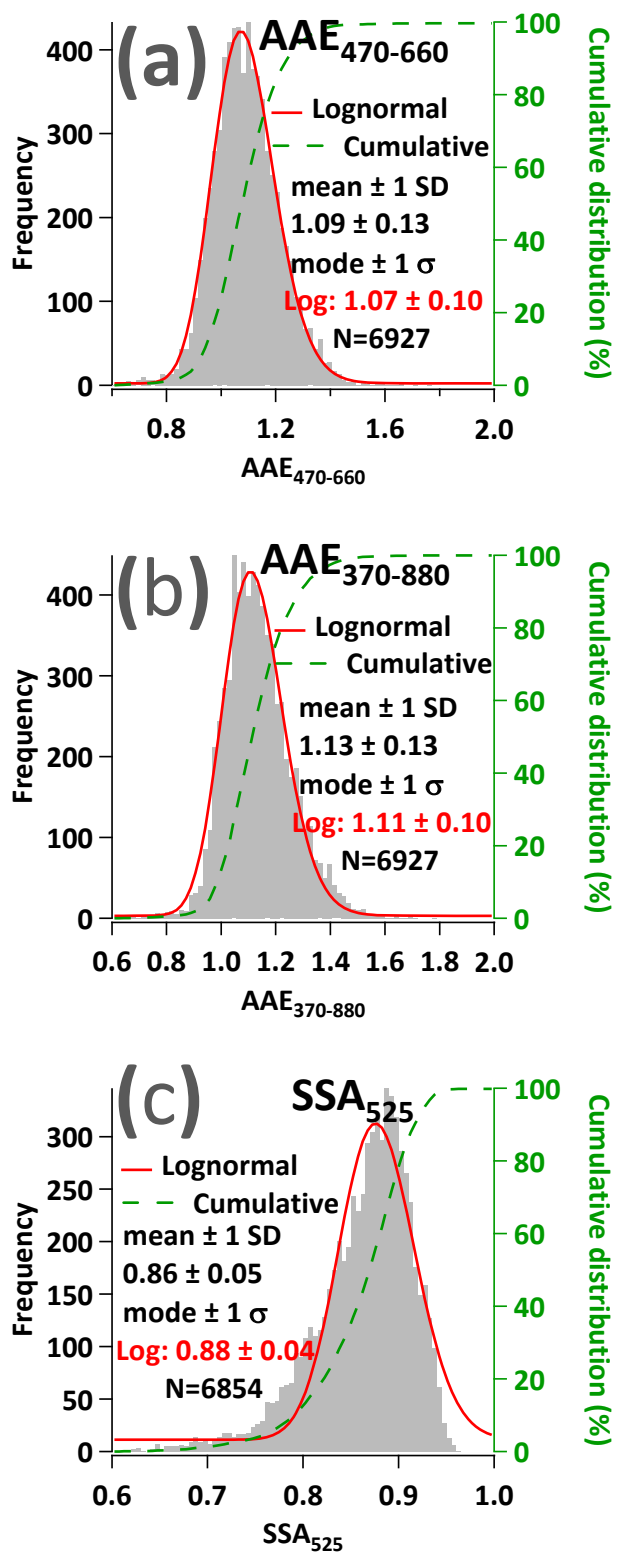
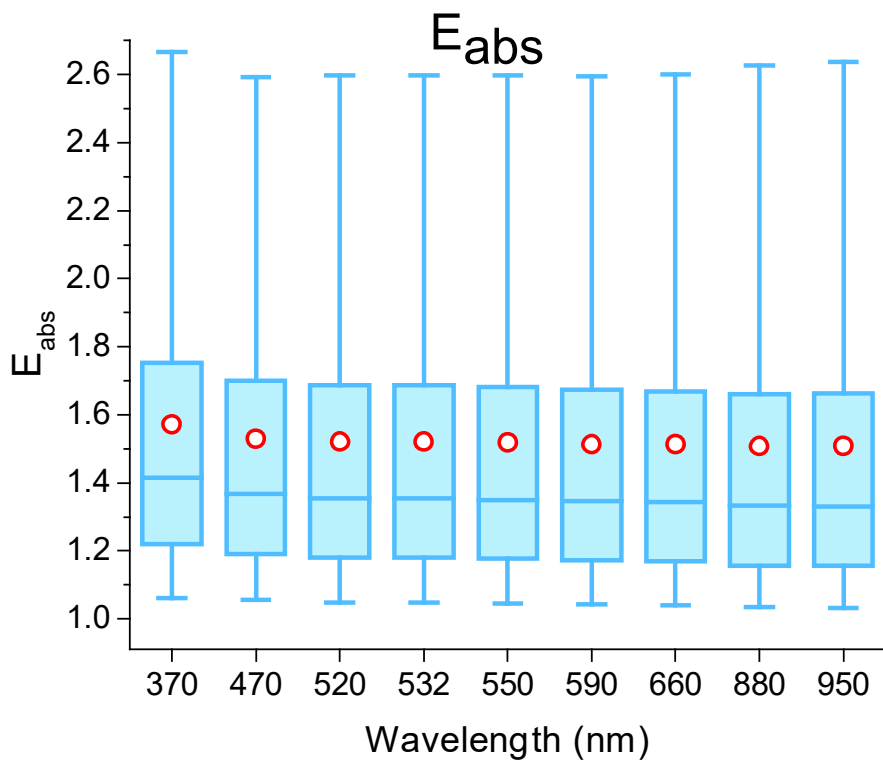


Figure S8. Measured annual statistics of AAE and SSA. (a) Annual frequency distribution of $\text{AAE}_{470-660}$. (b) Annual frequency distribution of $\text{AAE}_{370-880}$. (c) Annual frequency distribution of SSA_{525} . The red line represents lognormal fitting curve.



Wavelength (nm)	370	470	520	532	550	590	660	880	950
E_{abs} mean	1.55	1.51	1.50	1.50	1.50	1.49	1.49	1.48	1.49
E_{abs} S.D.	0.48	0.47	0.47	0.47	0.48	0.47	0.48	0.49	0.49

Figure S9. Spectrum annual average E_{abs} from 370 to 950 nm.

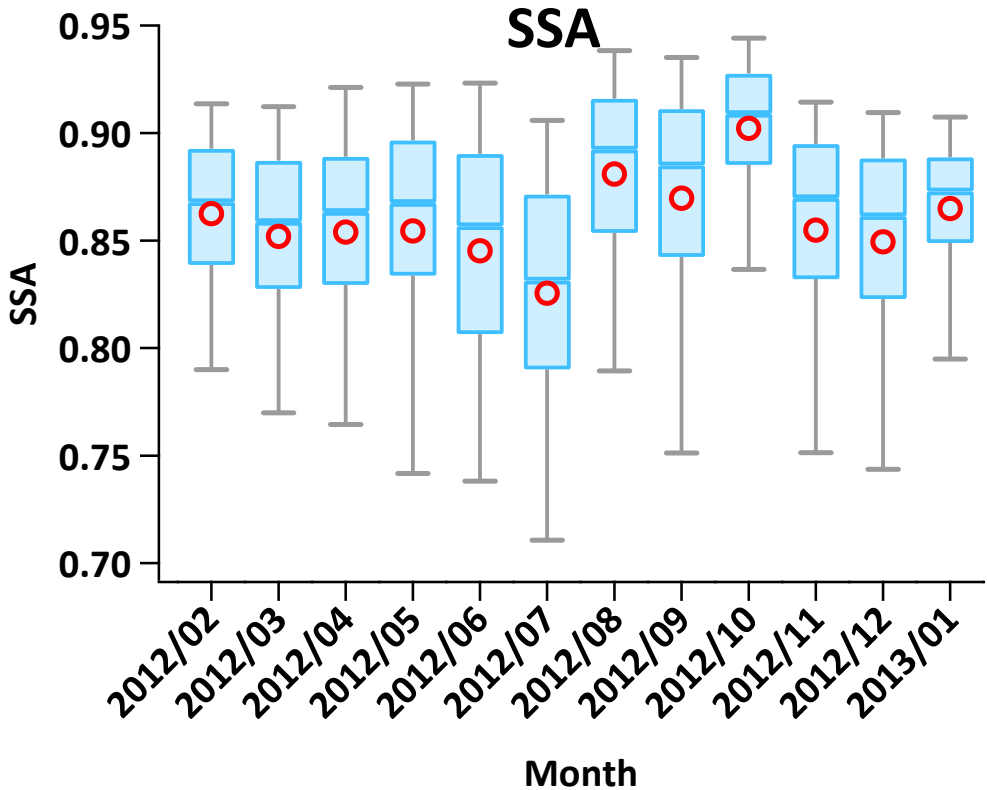


Figure S10. Measured monthly variations of SSA₅₂₅.

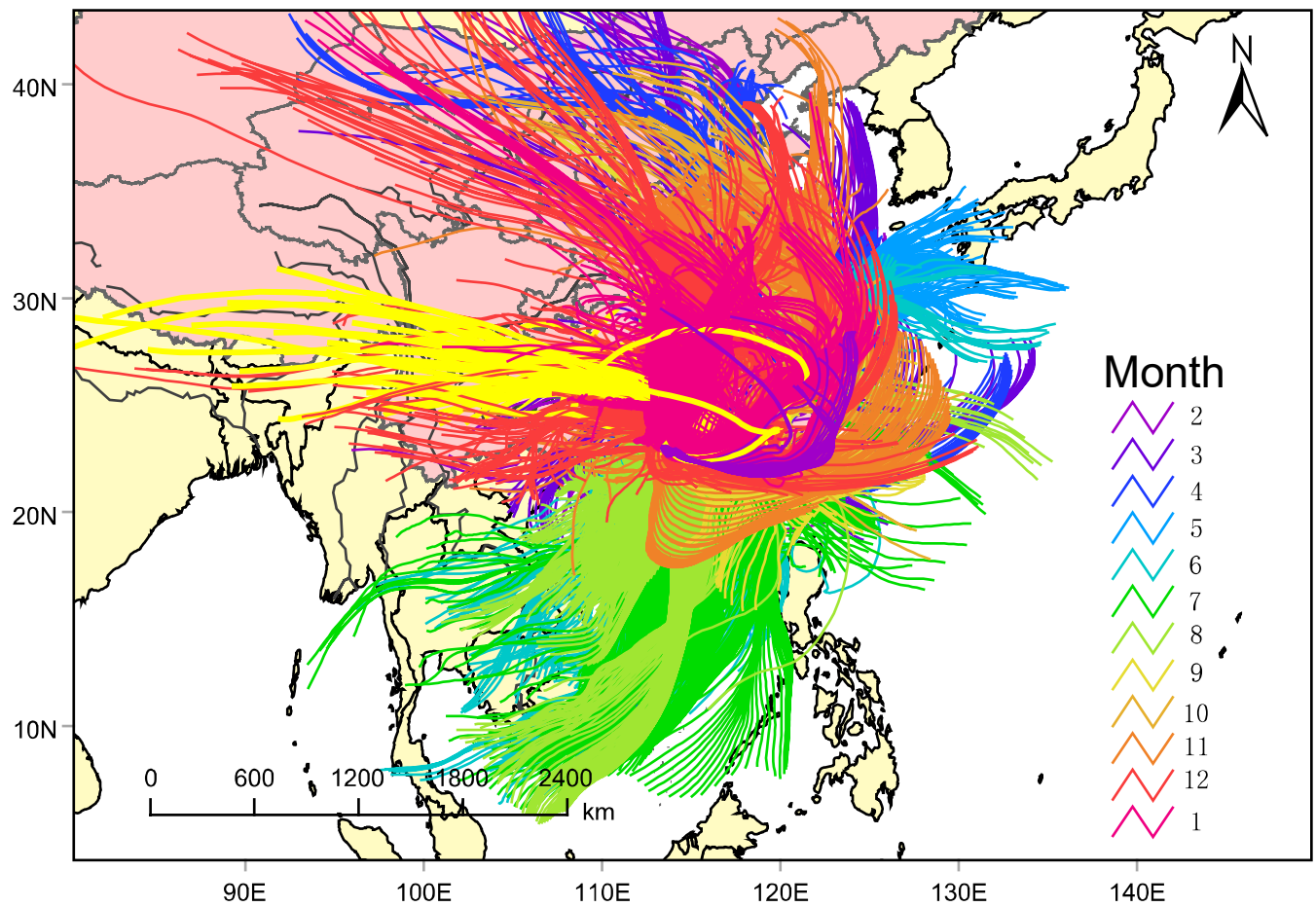


Figure S11. Hourly back trajectories for the past 72 hours calculated using NOAA's HYSPLIT model from Feb 2012 to Jan 2013. The color coding represents different months.

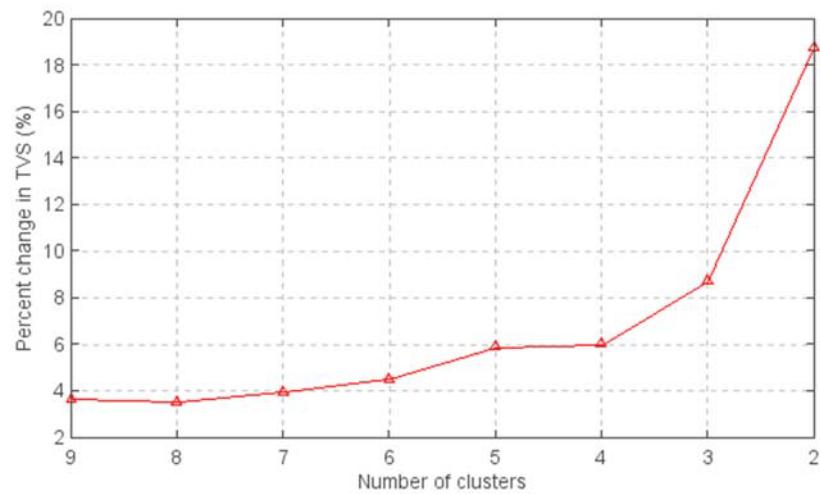


Figure S12. Total spatial variance (TSV) as a function of number of clusters in back trajectories clustering analysis.

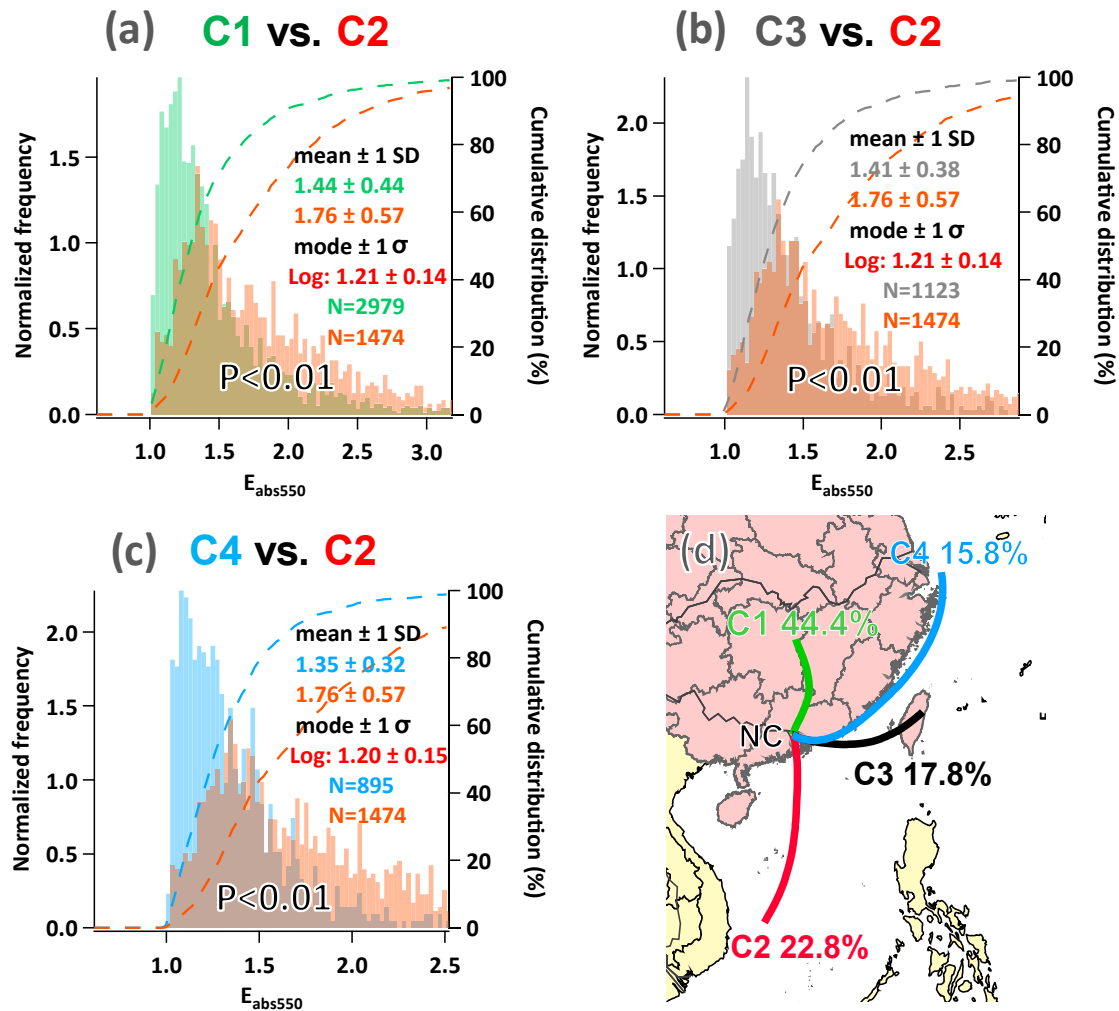


Figure S13. Frequency distributions of $E_{\text{abs}550}$ by different air mass clusters. P values are calculated from Wilcoxon-Mann-Whitney tests.

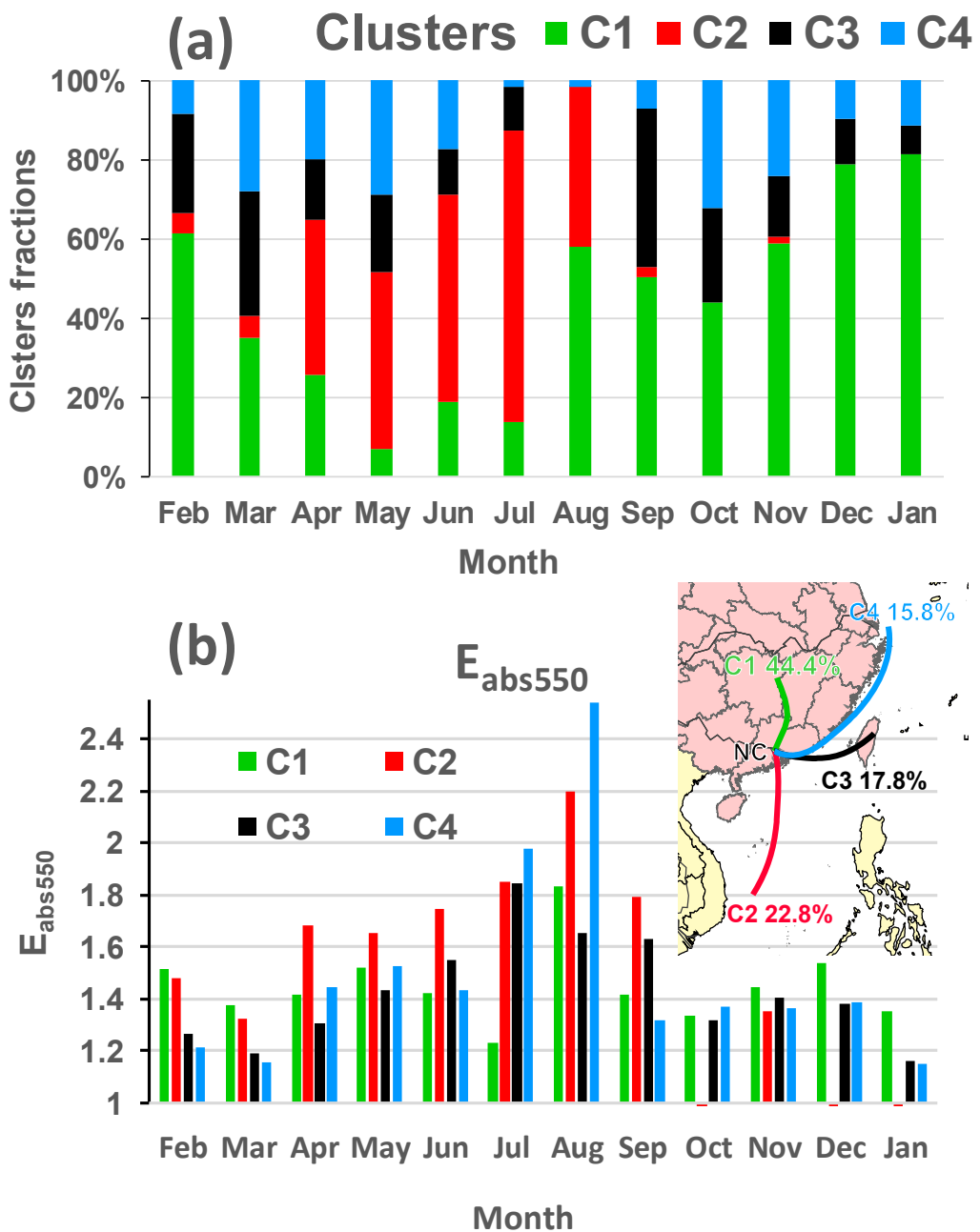


Figure S14. (a) Monthly contribution of each cluster. (b) Monthly E_{abs550} of each cluster.

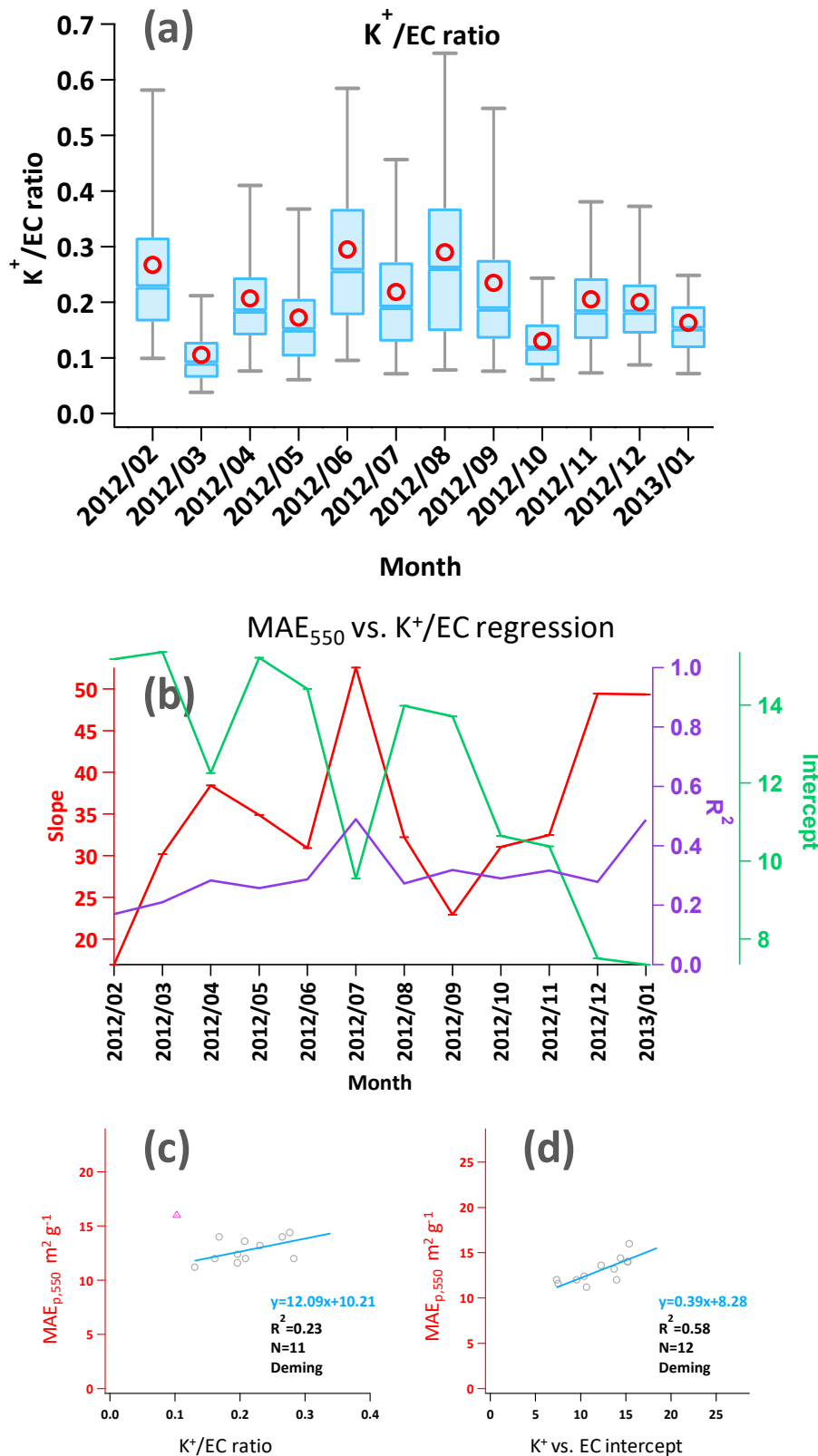


Figure S15. (a) Monthly variations of K^+/EC ratio from 2012 Feb to 2013 Jan at NC site. (b) Monthly regressions between MAE_{550} and K^+/EC with slope in red, intercept in green and R^2 in purple. (c) regressions between monthly $\text{MAE}_{p,550}$ and K^+/EC . (d) regression between monthly $\text{MAE}_{p,550}$ and intercepts from (b).

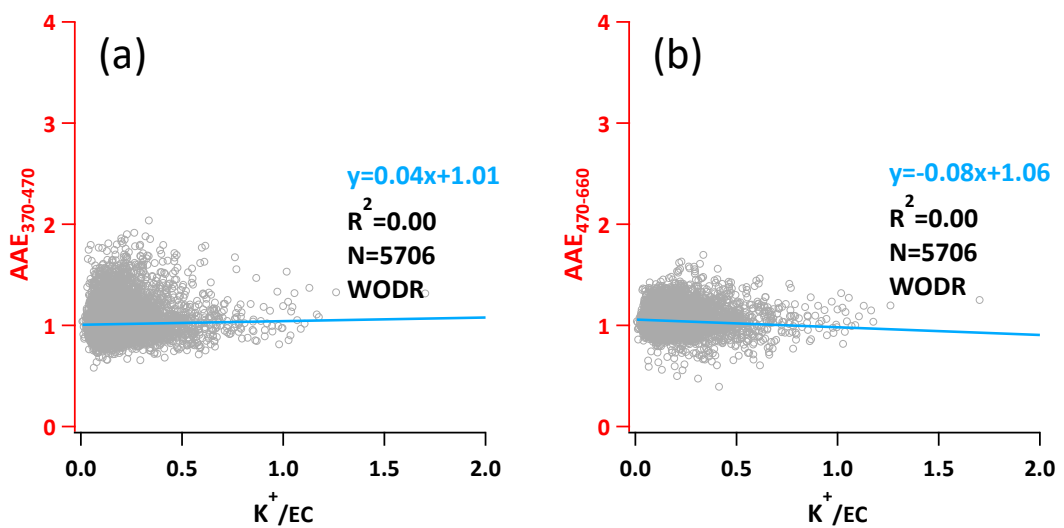


Figure S16. Correlations of AAE with K⁺/EC ratio (biomass burning indicator). (a) AAE from 370 – 470 nm. (b) AAE from 470 – 660 nm.

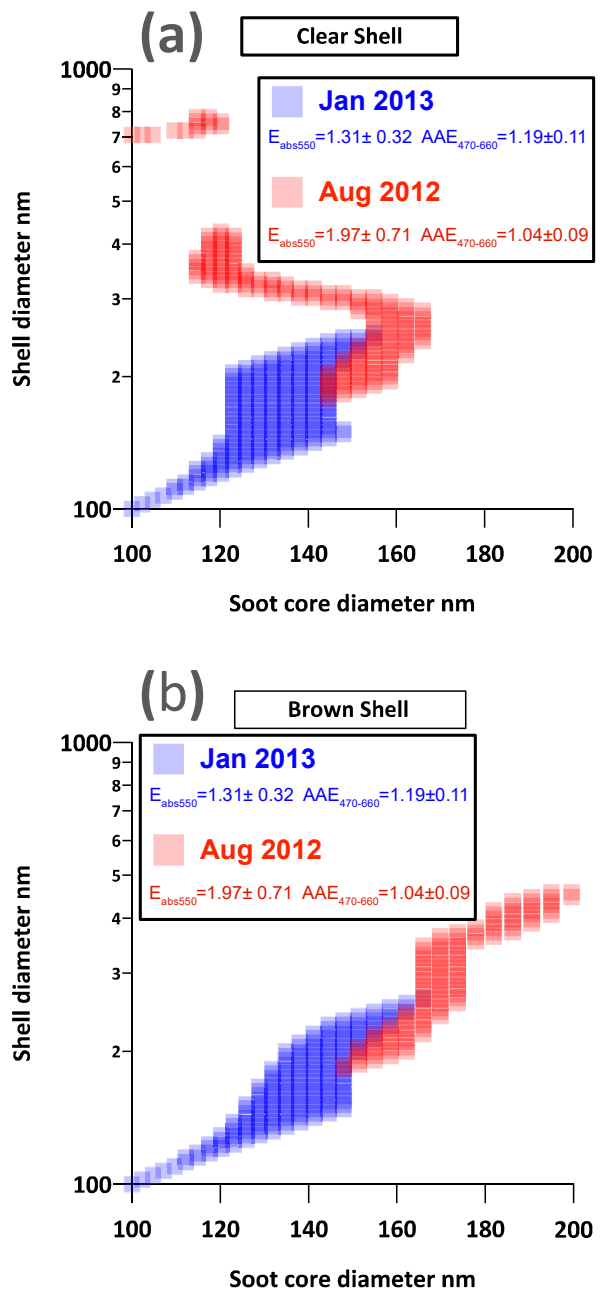


Figure S17. Size range of soot particles constrained by E_{abs} , SSA_{525} and $AAE_{470-660}$ from measurements. (a) Clear shell scenario; (b) Brown shell scenario

Test A

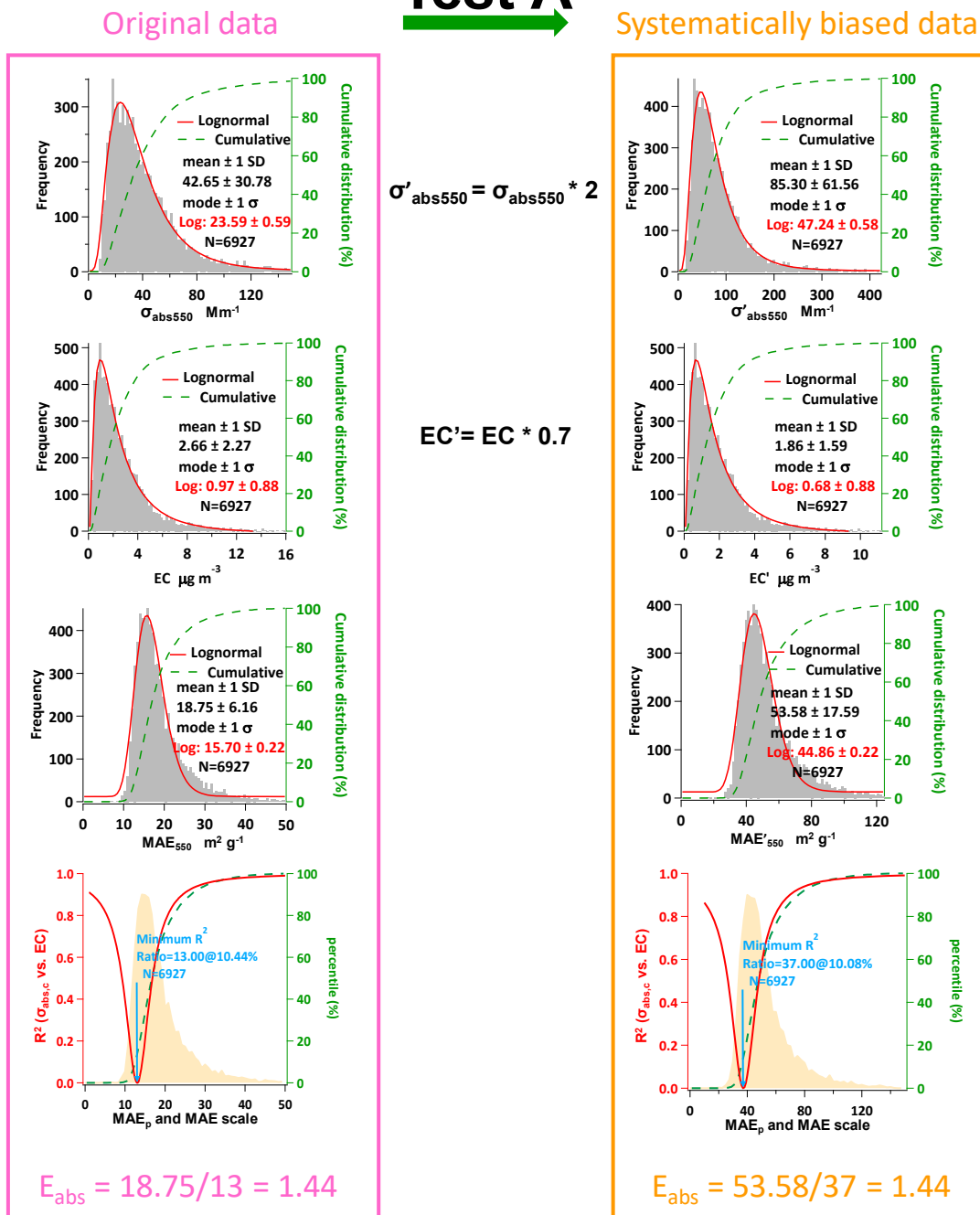


Figure S18. Comparison of E_{abs} from original data and systematically biased data (Test A). It should be noted that the E_{abs} shown here is ratio of averages, which is different form the annual average E_{abs} calculated from average of ratios.

Test B

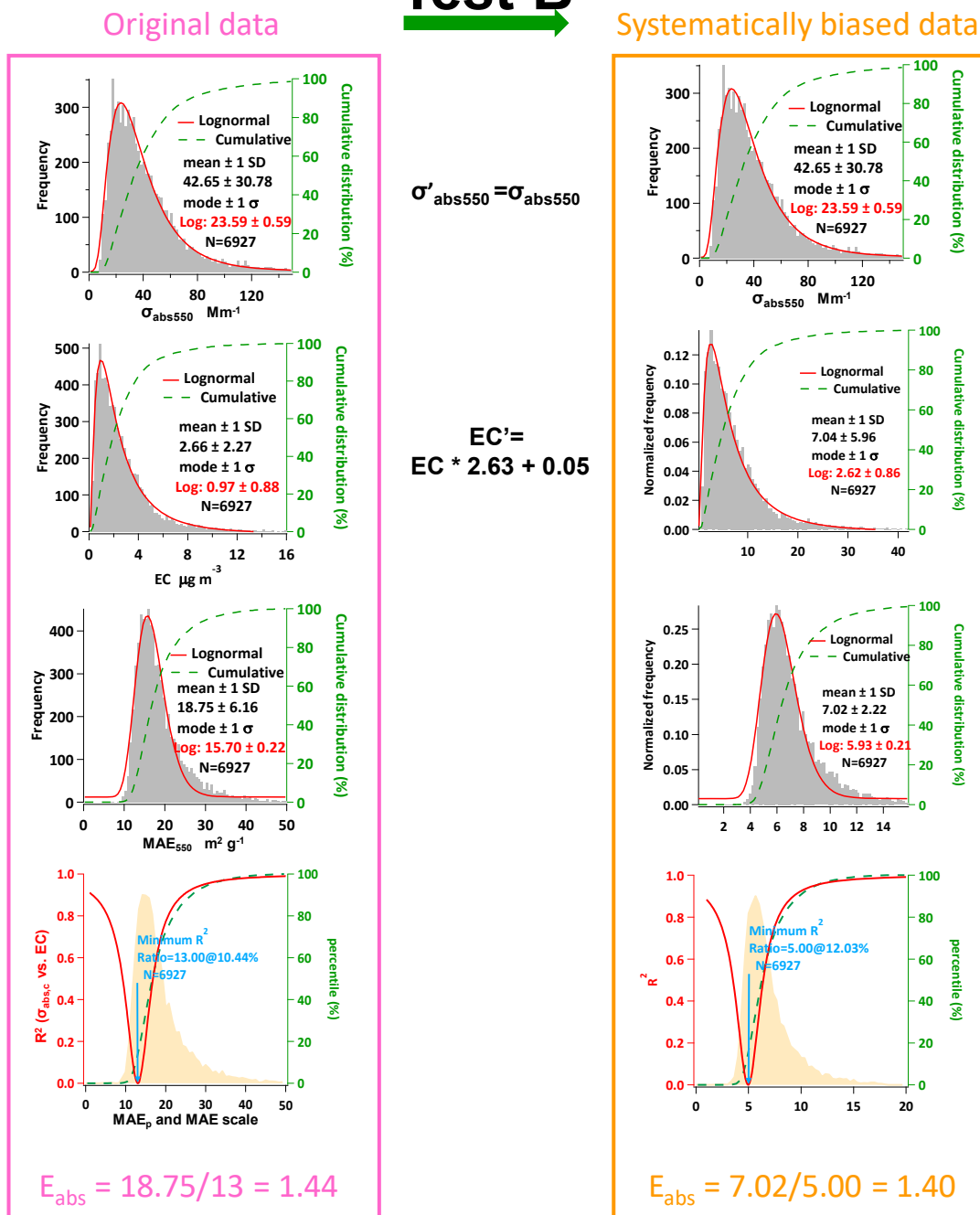


Figure S19. Comparison of E_{abs} from data using NIOSH EC and data using IMPROVE EC (Test B). It should be noted that the E_{abs} shown here is ratio of averages, which is different form the annual average E_{abs} calculated from average of ratios.

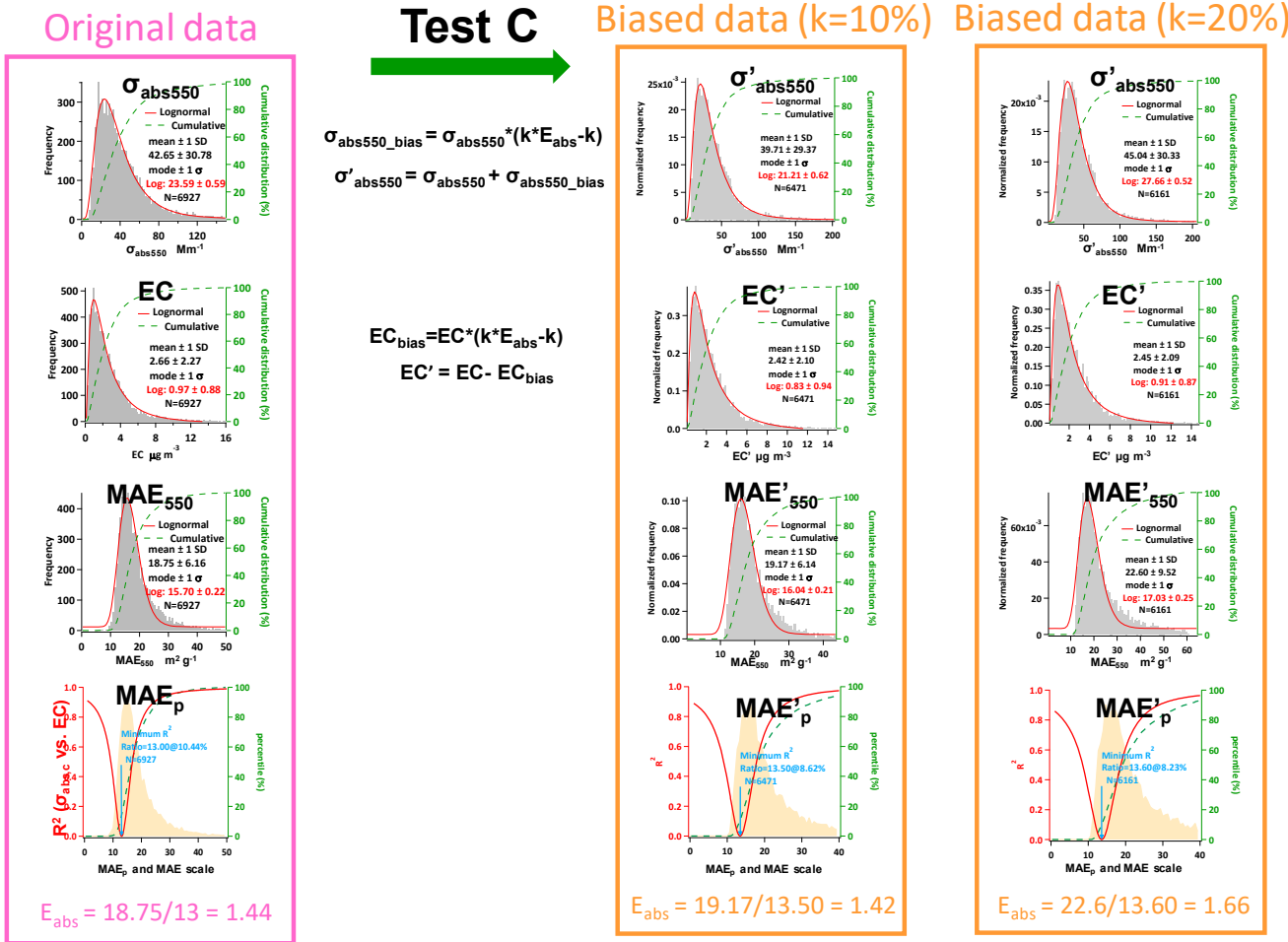


Figure S20. Comparison of E_{abs} from data using original data and E_{abs} depended biased data (Test C). It should be noted that the E_{abs} shown here is ratio of averages, which is different form the annual average E_{abs} calculated from average of ratios.

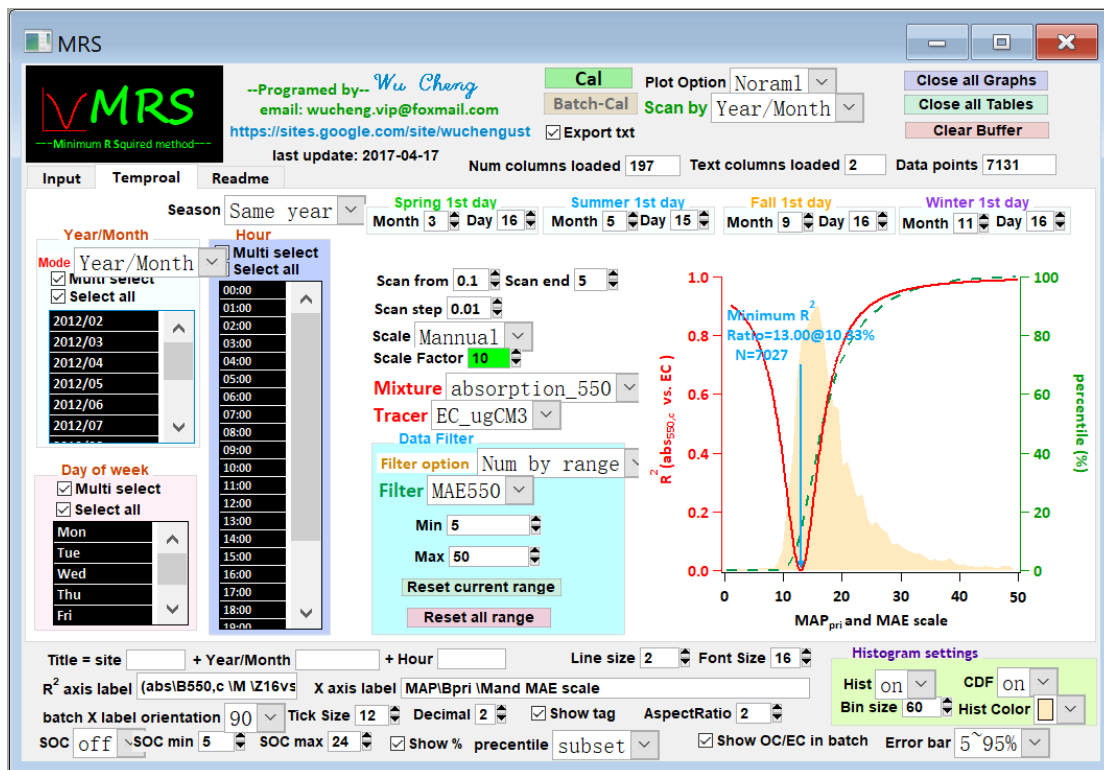
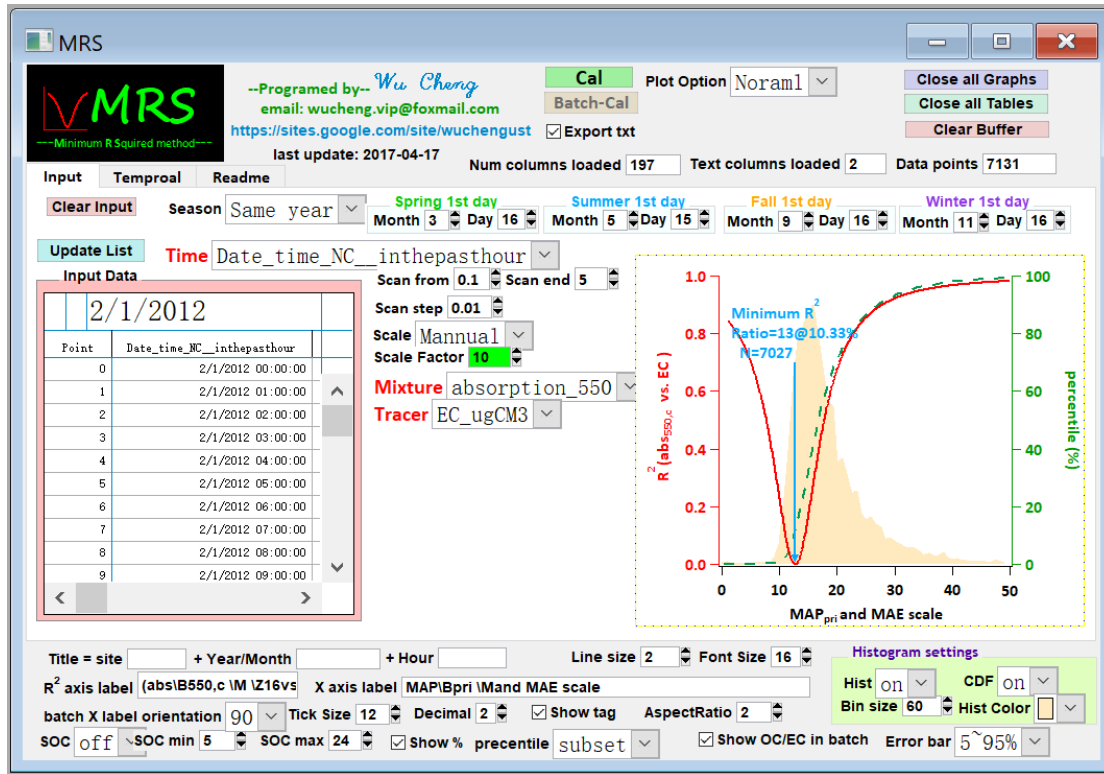


Figure S21. MRS program written in Igro Pro (WaveMetrics, Inc. Lake Oswego, OR, USA). Available from <https://sites.google.com/site/wuchengust>.

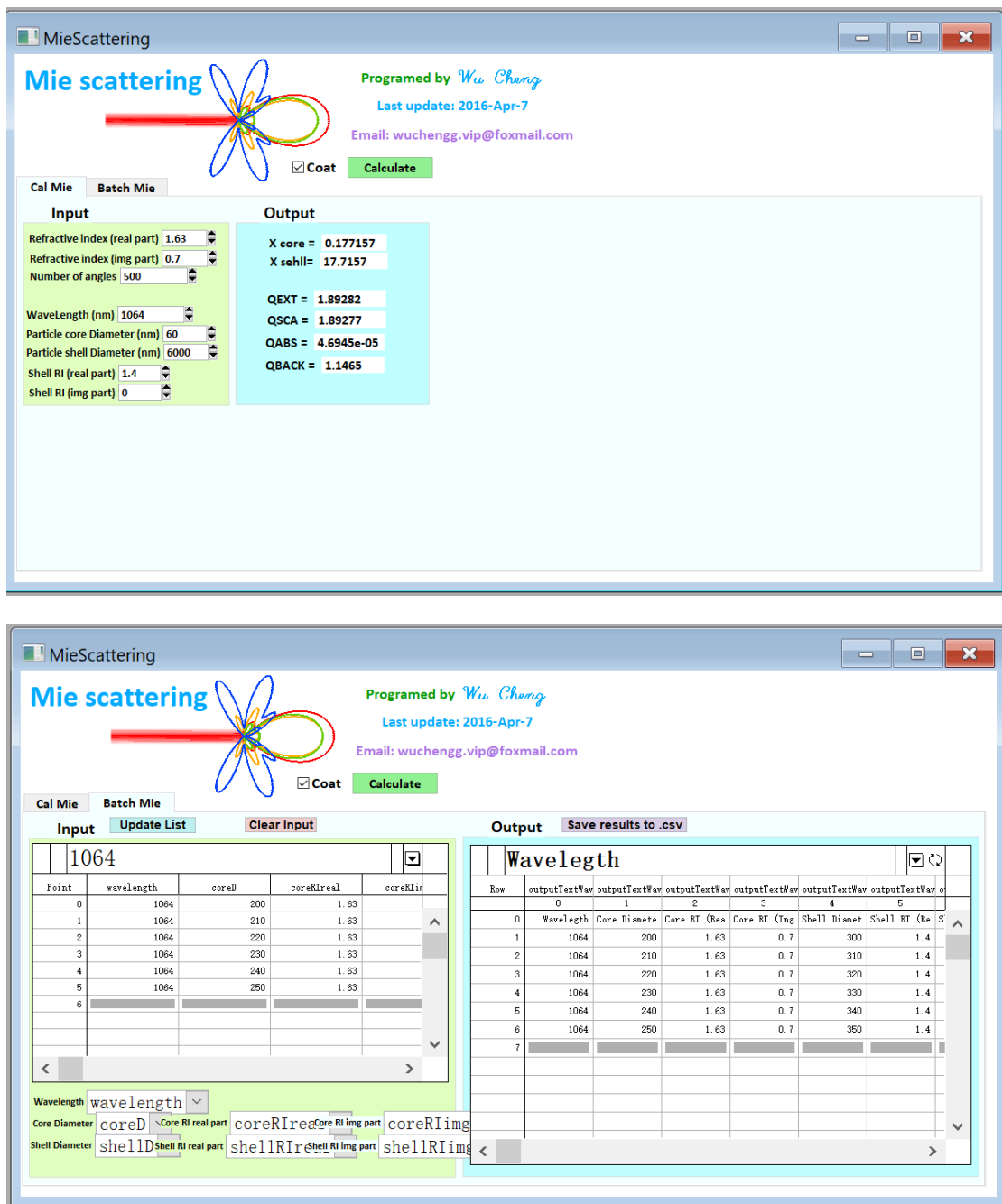


Figure S22. Mie program written in Igro Pro (WaveMetrics, Inc. Lake Oswego, OR, USA). Available from <https://sites.google.com/site/wuchengust>.

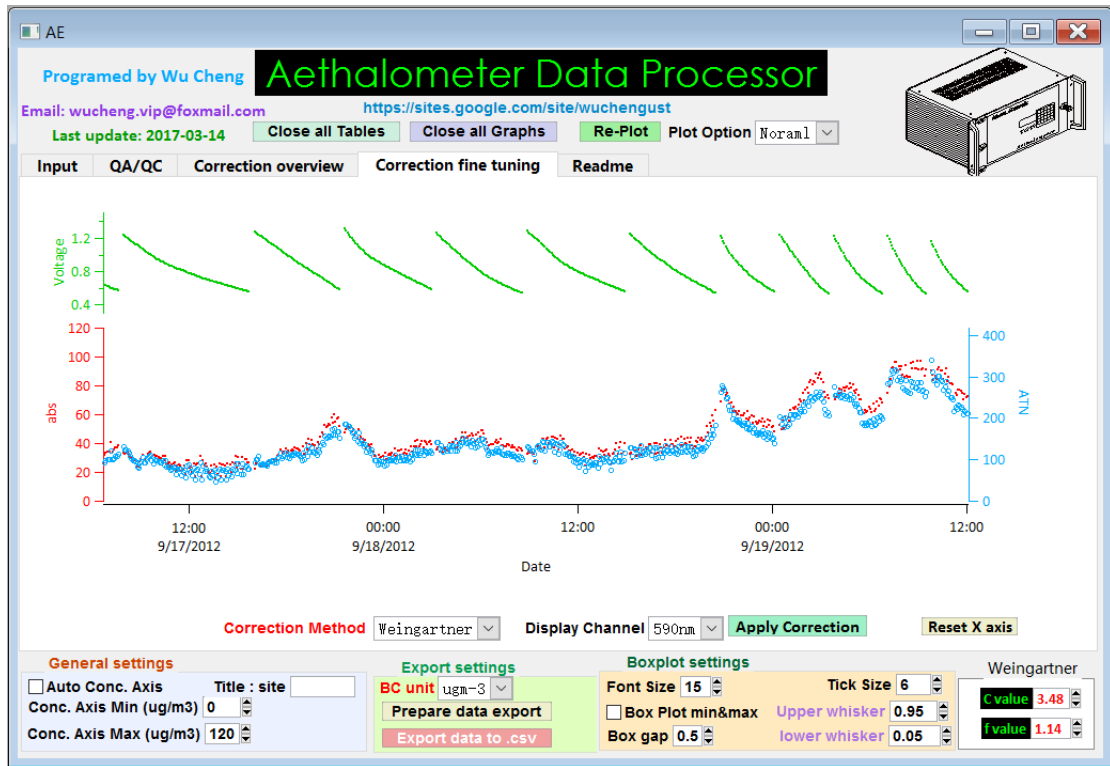
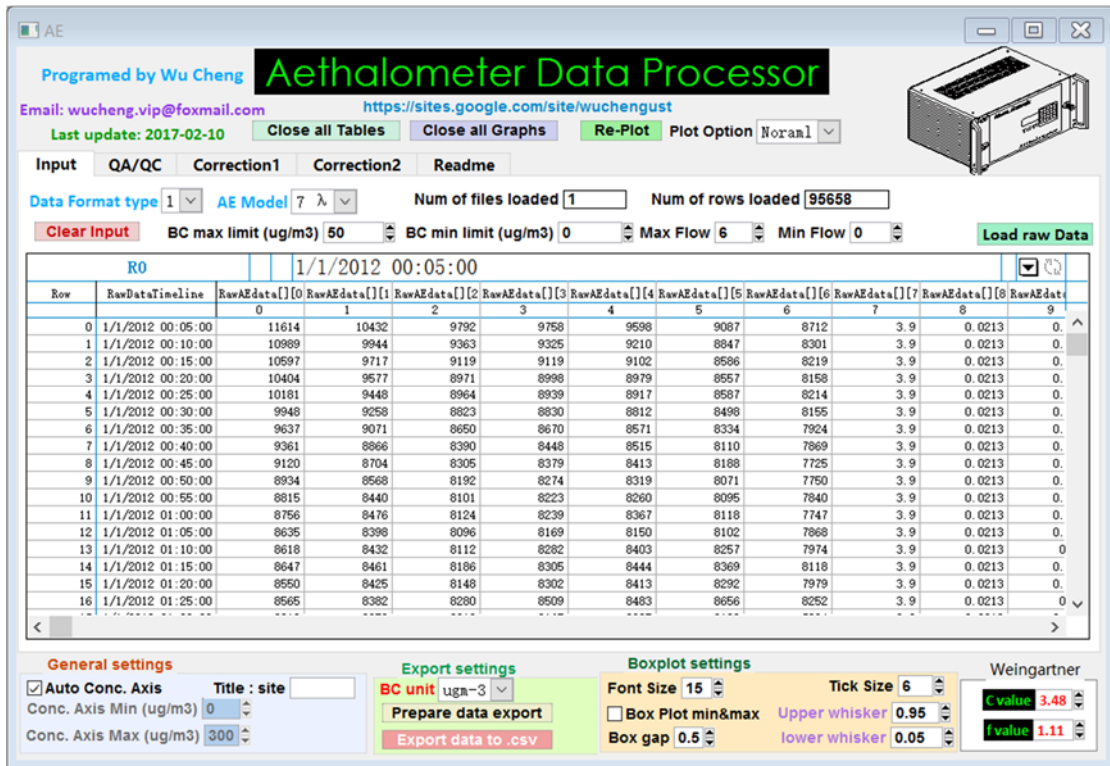


Figure S23. Aethalometer data processing program written in Igro Pro (WaveMetrics, Inc. Lake Oswego, OR, USA). Available from <https://sites.google.com/site/wuchengust>.

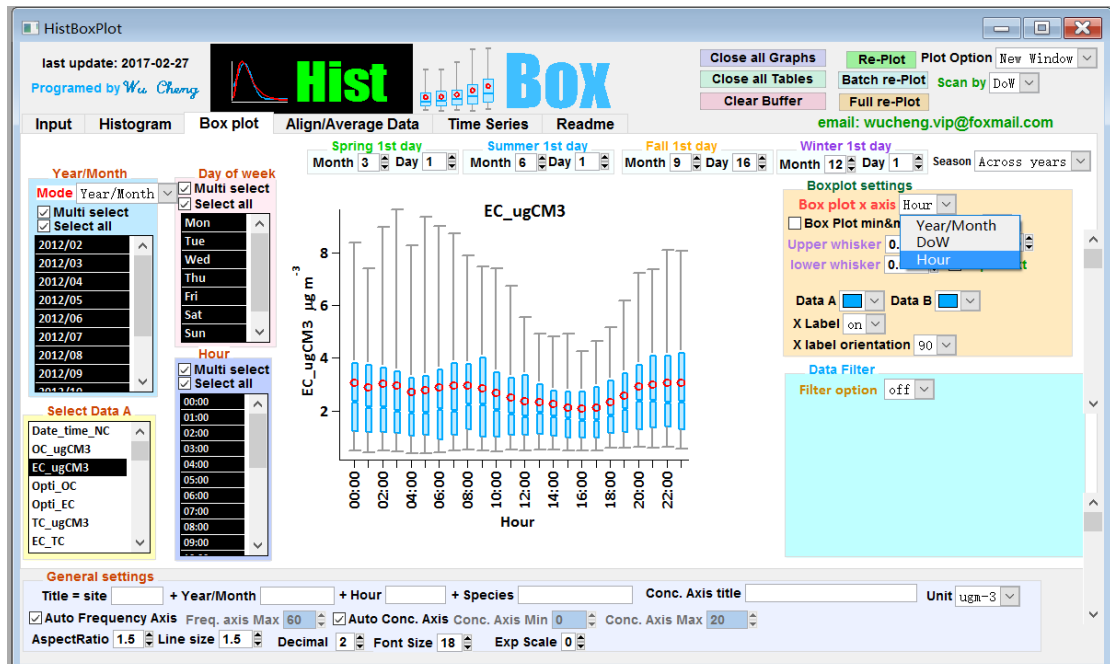
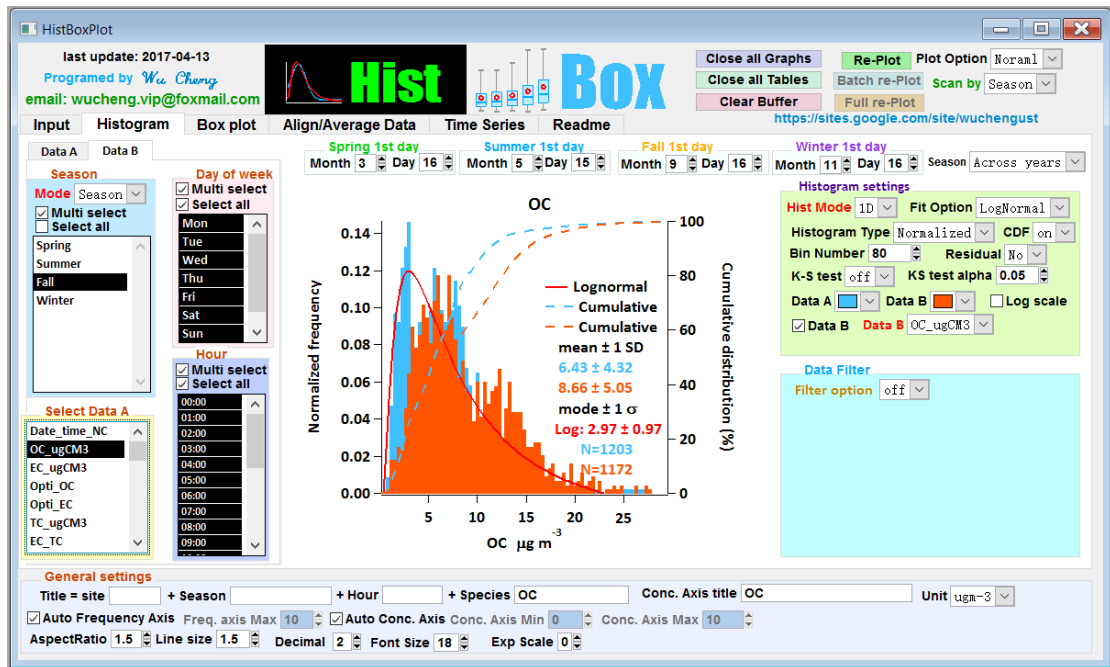


Figure S24. Histbox program written in Igro Pro (WaveMetrics, Inc. Lake Oswego, OR, USA). Available from <https://sites.google.com/site/wuchengust>.

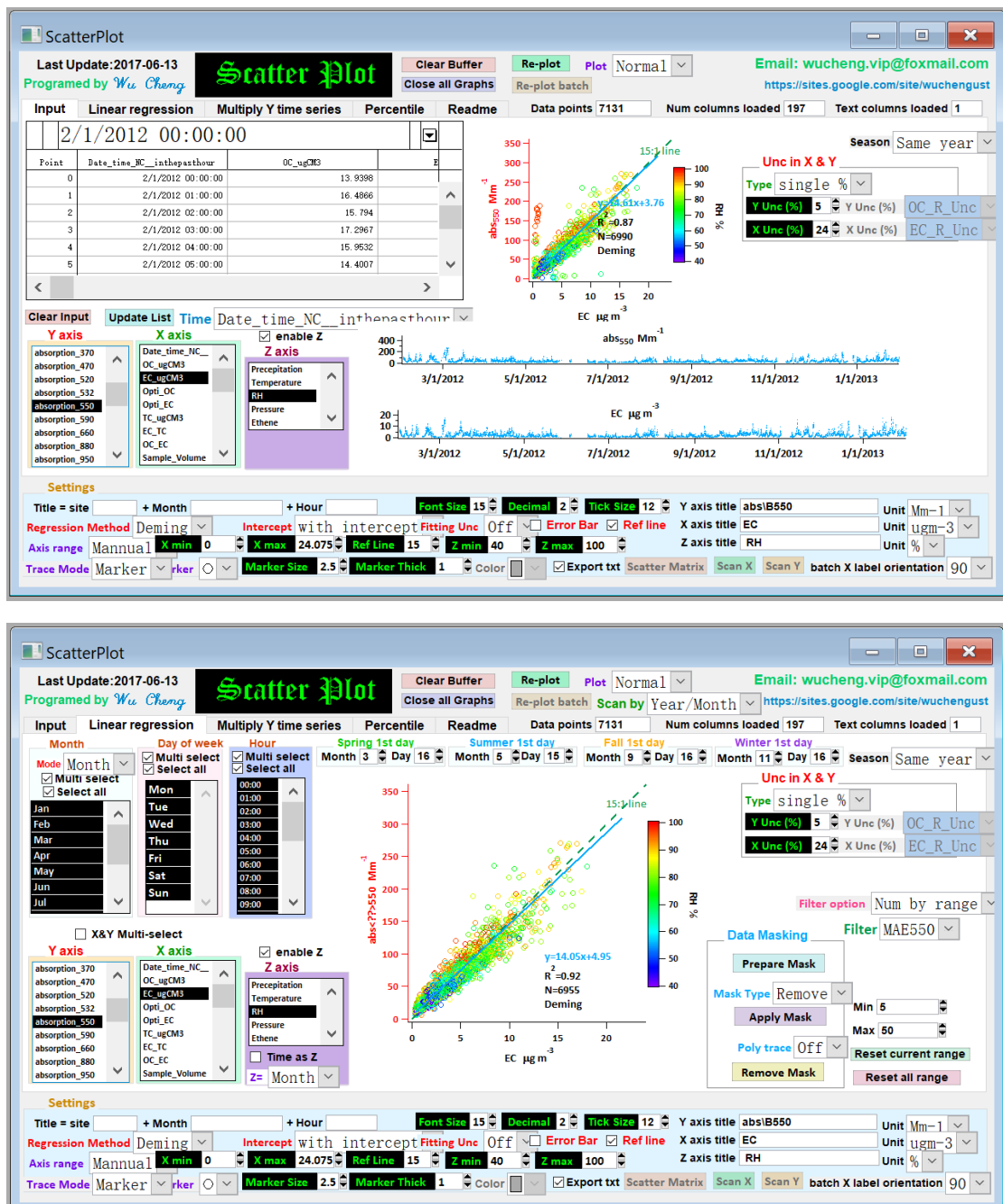


Figure S25. Scatter plot program written in Igro Pro (WaveMetrics, Inc. Lake Oswego, OR, USA). More details can be found in a separated paper (Wu and Yu, 2017). Available from <https://sites.google.com/site/wuchengust>.